ACS OMEGA

Article

Cite This: ACS Omega 2018, 3, 10631−10637

http://pubs.acs.org/journal/acsodf

Nanoparticles Self-Assembly within Lipid Bilayers

Henry Chan*,†,∥ and Petr Král*,†,‡,§

†Department of Chemistry and ‡Department of Physics, University of Illinois at Chicago, 845 W Taylor Street, Chicago, Illinois 60607, United States

§Department of Biopharmaceutical Sciences, University of Illinois at Chicago, 833 S Wood Street, Chicago, Illinois 60612, United States

ABSTRACT: Coarse-grained molecular dynamics simulations are used to model the self-assembly of small hydrophobic nanoparticles (NPs) within the interior of lipid bilayers. The simulation results reveal the conditions under which NPs form clusters and lattices within lipid bilayers of planar and spherical shapes, depending on the NP−lipid coupling strengths. The formation of nanopores within spherical bilayers with self-assembled planar NPs is also described. These observations can provide guidance in the preparation of functional bio-inorganic systems.

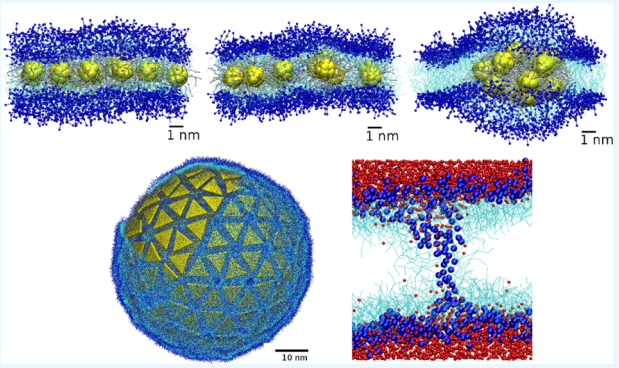

1. INTRODUCTION

Many natural superstructures are formed by self-assembled lipids, peptides, proteins, polynucleotides, and other molecules.[1] These natural systems have inspired the preparation of materials composed from self-assembled synthetic nanoscale components, such as nanoparticles (NPs), block copolymers, and graphene.[2−7] Such granular materials can possess highly tunable properties, which depend on the sizes, shapes, and surface chemistries of the self-assembled nanoscale components. Complexation of biomolecules with nanoscale components can produce hybrid materials,[8] suitable for molecular sensing, drug delivery, filtration/separation, and medical imaging.[9−15]

Recently, hybrid NPs-lipids superstructures have been prepared. For example, NPs with hydrophobic ligands can form hybrid Janus vesicle-NPs structures.[16−18] Superparamagnetic iron oxide NPs embedded within lipid vesicles can be used as drug carriers and site-specific contrast agents in magnetic resonance imaging.[19] NPs of different sizes and surface properties can disrupt lipid bilayers[20,21] and change their permeability,[22,23] phase transition points,[24,25] and mechanical responses.[26]

The development of hybrid materials requires a good understanding of complex interactions of biomolecules and inorganic colloidal NPs.[27] Molecular dynamics (MD) simulations can be used to describe NPs self-assembly processes during the formation of materials.[28,29] Coarse-grained (CG) MD simulations can describe particularly large systems, since they map groups of atoms on CG beads. For example, CGMD simulations have been used to describe translocations of NPs and fullerene through lipid bilayers.[30−35] Small gold NPs coated with a mixture of anionic and hydrophobic ligands can translocate through lipid membranes without breaking them down.[36−41] These studies have also shown that NPs can adsorb onto or embed within bilayer membranes depending on their sizes, shapes, and surface properties. Furthermore, the composition, distribution, and flexibility of ligands on NP surfaces can influence their translocation behavior.[42−44] These studies model the insertion and stabilization of individual NPs inside lipid bilayers, however, there are relatively few studies that focus on the synergetic assembly of NPs and lipids in the context of biohybrid systems, such as the self-assembly of NP chains and nanoshells guided by lipid membranes.[45−47] In particular, the self-assembly of NP clusters within lipid bilayer has so far not been simulated.

Here, we model hybrid systems formed by superlattices of small hydrophobic NPs inside lipid bilayers.[48−51] These complex systems resemble other self-standing NPs membranes.[52−54] The goal of this study is to understand the conditions under which NP clusters insert into lipid bilayers, stabilize within them, and form superstructures. We also study how NPs of different shapes, sizes, and chemistries affect the lipid bilayers, in particular, create pores in the bilayers.

2. RESULTS AND DISCUSSION

2.1. NP Insertion into Lipid Bilayers. First, we simulate the insertion of a single NP into a lipid bilayer, in analogy to graphene insertion into lipid bilayers.[8] Small NPs with hydrophobic ligands can enter lipid bilayers due to a favorable coupling between their ligands and lipid tails,[16] as observed in recent experiments.[55] The hydrophobic NP is initially solvated

Received: June 25, 2018
Accepted: August 23, 2018
Published: September 5, 2018

DOI: 10.1021/acsomega.8b01445
ACS Omega 2018, 3, 10631−10637

in water within a micelle formed by lipid molecules. The density of lipids in the micelle determines the NP solubility in water, which affects its ability to enter the lipid bilayer.

To study the NP insertion dynamics, we first prepared a 13 × 13 nm^2 1-palmitoyl-2-oleoyl-*sn*-glycero-3-phosphocholine (POPC) bilayer and equilibrated it in water with no external lateral tension. The equilibrated bilayer has a thickness of h_{mem} ≈ 5 nm and a lipid density of d_{mem} ≈ 2 lipids/nm^2. A single small (d = 1.6 nm) hydrophobic NP covered by different numbers of solvation lipid molecules is placed in water, about 0.1−0.2 nm above the equilibrated POPC bilayer. These solvation lipid molecules are the same as those in the bilayer. The coverage of solvation lipids around the NP within the solution is quantified by a ratio of $R_c = N_{lip}/N_{lig}$, where N_{lip} is the number of solvation lipid molecules around the NP and N_{lig} = 42 is the number of NP ligands. We did not observe detachment of lipids from the NP during the simulations.

Figure 1a−d shows the insertion of a hydrophobic NP with a high lipid coverage (R_c = 2.6). The insertion dynamics closely resembles a fusion of lipid vesicles.[56] At t = 0 ns (beginning of the insertion), the NP-micelle is in close contact with the surface of the POPC bilayer, maintained by the coupling between amine and phosphate lipid head groups (Figure 1a). The contact area directly below the NP becomes flat, which introduces strain onto the lipid molecules around it. The strained regions of the bilayer eventually rupture and expose the NP ligands to the hydrophobic interior of the lipid bilayer (Figure 1b). Figure 1f shows the ruptured region of the micelle at the bottom of the NP above the lipid bilayer. The NP initially interacts only with the top lipid layer, and the bottom lipid layer responds to the movement of the top lipid layer. However, as the ruptured region of the bilayer slowly expands, the NP ligands penetrate the top lipid layer and start to interact with lipid tails in the bottom leaflet of the lipid bilayer (Figure 1c), which creates a distinct inverted funnel-shape structure below the NP. At t = 84 ns, the NP is inside the bilayer, and the funnel structure starts to recede (Figure 1d). The stabilization of the inserted NP within these asymmetrical lipid layers can take another ≈100 ns. The flip-flop motion of lipids between the top and bottom leaflets of the bilayer is expected to restore the symmetry of the bilayer over microsecond to millisecond timescale.

The initial coverage of lipids around the NP determines the time it takes the NP to intercalate within the lipid bilayer. We can define an insertion time, t_{in}, as the time from the NP penetration of the top leaflet till its full stabilization within the bilayer. Figure 1e shows the dependence of t_{in} on the lipid coverage ratio, R_c. When the lipid coverage is relatively low ($R_c \leq 1$), the insertion time is constant, $t_{in} \approx 6.5$ ns, where the NP insertion involves an abrupt penetration of the top bilayer leaflet. Rapid penetration of NP through the lipid layer is driven by a minimization of water surface tension (hydrophobic interactions). When $R_c > 1$, the insertion mechanism follows the previously described fusion of lipids. The growth of t_{in} with R_c is due to an increased density of lipids on the NP surface, which gives a more stable micelle within the water solvent. Figure 1h,i shows a significant change in the angle distribution of these lipid molecules before the insertion (red) and after (green) as compared to a normal bilayer (blue). In the simulations, we observe coupling between polar head groups of the bilayer and a NP-micelle even for a full lipid coverage ($R_c > 3$), as shown in Figure 1g. However, these closely packed lipids prevent the formation of a strained flat surface that is needed to initiate membrane rupturing of the NP insertion process.

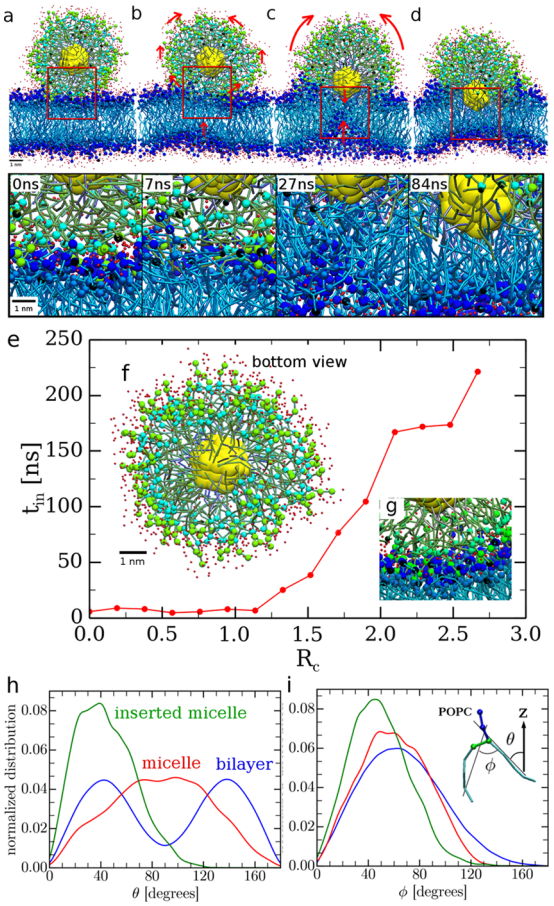

Figure 1. (a−d) Snapshots and close-up views of the first 84 ns of a NP inclusion process. Arrows indicate the motion of NP and lipid molecules. Initially, the NP is covered with 112 solvation lipids (R_c = 2.6), which are colored in green to distinguish them from those of the bilayer. Nearby water molecules are shown in red. (e) The inclusion time of NP with different coverages of solvation lipids. (f) A bottom view of the NP at t = 7 ns, which shows an opening of the structure due to bottom-to-top motion of lipid molecules. (g) A close-up view of the stable contact between polar head groups of the structure and those of the bilayer. This NP is solvated by 126 lipid molecules (R_c = 3.0), and it does not penetrate the bilayer within our simulation time. (h, i) Tilt angle analysis of the solvation lipid when R_c = 1.33. Normalized distributions of an azimuthal tilt angle and an angle between hydrophobic tails of POPC lipid molecules.

2.2. Equilibrium NP−Lipid Superstructures. Next, we investigate how small hydrophobic NPs (d = 1.6 nm) self-assemble once they enter the lipid bilayer. In general, their equilibrium arrangement depends on the NP−NP, NP−lipid, and lipid−lipid coupling strengths, NP shapes, and other parameters. We first model NPs with variable NP−NP coupling strengths, while keeping the other coupling strengths fixed. The relative coupling strengths between NPs are scaled by a factor of $\alpha = \epsilon_1/\epsilon_0$, where ϵ_1 is the modified strength of the C_1S-C_1S (NP−NP) Lennard-Jones (LJ) coupling and ϵ_0 is the original strength of C_1S-C_1S LJ coupling, equivalent to the C_1S-C_1 (NP−lipid) and C_1-C_1 (lipid−lipid) LJ coupling strengths. Different NP−lipid structures are observed, depending on the NP−NP coupling strength (α = 0.5, 1.0, and 1.5) and the number of lipids present in the system.

DOI: 10.1021/acsomega.8b01445
ACS Omega 2018, 3, 10631−10637

For a small number of lipids (≈452), a 13 NP cluster forms a compact cluster when $\alpha > 1$ or it reorganizes into a small liposome from a micelle-coated NP cluster (Figure 2a) when α = 0.5. The equilibrated liposome structure is similar to Janus-NP vesicles.[16] Such structure is more stable for weakly coupled NPs, since it maximizes the amount of coupling between NP ligands and lipid tails. In our simulations, we observed about a dozen of water molecules entering the hydrophilic interior of the liposome during the liposome reorganization process.

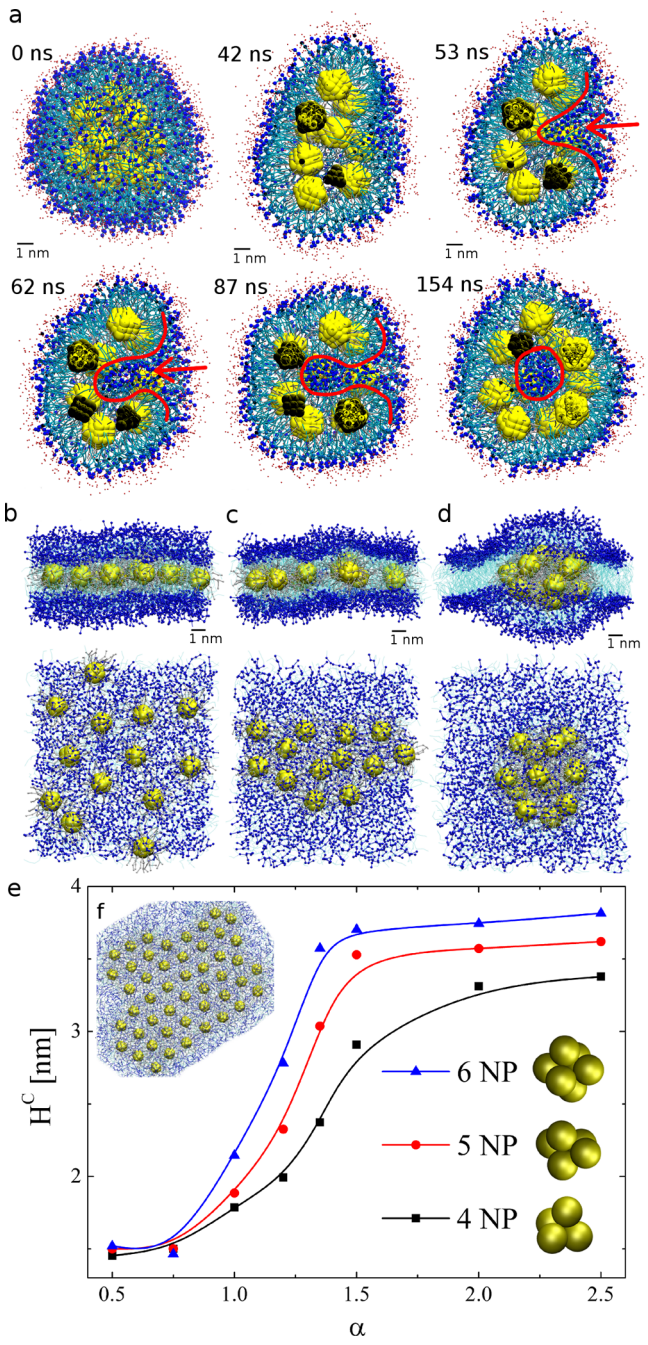

Figure 2. (a) Reorganization of lipid molecules in a liposome carrying 13 NPs with α = 0.5. (b–d) Stabilization of 13 NPs within a lipid bilayer: (b) α = 0.5 after 125 ns, (c) α = 1.0 after 814 ns, (d) α = 1.5 after 359 ns. (e) The height of small NP clusters, $h_C(\alpha)$. (f) Hexagonal arrangement of 48 hydrophobic NPs with α = 1 equilibrated in the lipid bilayer for 500 ns.

These results show that how nanosize vesicles could be prepared by designing NPs with hydrophobic ligands having NP–NP interactions weaker than NP–lipid interactions (possibly by adjusting the length of alkyl NP ligands) and allowing a cluster of such NPs to self-assemble with lipids. These vesicles can potentially be designed for use as transport cargo in biological systems. Such vesicles are difficult to prepare in experiments due to the strain induced by the formation of a large surface curvature.

When the lipids form a bilayer, a 13 NP cluster within it can form a loose monolayer (Figure 2b) when α = 0.5, a close-packed monolayer (Figure 2c) when α = 1, or a compact globular cluster (Figure 2d) when α = 1.5. To better understand this self-assembly behavior, NP clusters formed of 4 (tetrahedron), 5 (trigonal bipyramid), and 6 (octahedron) NPs with α = 0.5–2.4 are simulated inside a lipid bilayer. We calculated the average height of the equilibrated NP cluster, h_C, by subtracting the z-coordinate of the bottom-most SC_4 CG beads from top-most SC_4 CG beads. Figure 2e shows a plot of h_C as a function of α, averaged over the last 75 ns of the $t \approx$ 250 ns long simulations. NPs in larger clusters (5, 6 NPs) have more contact points with each other, which leads to stronger clusters that flatten only at smaller α. Similar to the 13 NP clusters shown in Figure 2b–d, all of these clusters flatten at $\alpha \leq 1$ to a loose or compact monolayer with a hexagonal close-packed arrangement. Figure 2f shows a fully equilibrated monolayer of initially scattered 48 NPs with α = 1.

The results in Figure 2 can be better understood if we realize that bilayer membranes are stabilized through a balance of positive and negative lateral tensions, generated by the different molecular groups present at different heights.[57,58] At equilibrium, the net lateral tension is close to zero. However, this balance is changed when the bilayer is deformed by the inserted NPs, leading to local tensions caused by the exposure of hydrophobic groups in curved lipid membranes.[59] This local tension generates a net vertical force on the inserted NP cluster (flattening), which determines its equilibrium height, h_C. Therefore, NP clusters can be formed from coalescence of individually inserted NPs or from the direct insertion of a NP cluster into the lipid bilayer. The lateral and vertical sizes, as well as the overall shapes, of the equilibrated NP clusters within the superstructure correlate to the border surface tension of the lipid layers.

2.3. Stabilization of Nanodiscs (NDs) in Liposomes.

Hybrid superstructures might be also formed within curved bilayers, such us liposomes. To examine this possibility, we prepared equilateral triangular nanodiscs (NDs) with a side length of $l_{ND} \approx$ 7.2 nm and a thickness of $h \approx$ 0.6 nm; Gd_2O_3 nanoplates[60] and triangular gold nanodiscs[61] have been prepared experimentally.[62−65] These triangular NDs were arranged into groups of 6 and 5 to form larger hexagonal and pentagonal plates. Using 180 NDs arranged into 20 hexagons and 12 pentagons on a sphere and coated with (36 748) lipid molecules in water, we prepared a large truncated icosahedron shape liposome structure (Figure 3a), resembling a fullerene. Self-assembled hexagons have a zero curvature (planar), whereas self-assembled pentagons provide a positive curvature, necessary for the formation of a spherical polyhedra. Note that other convex polyhedrons satisfying the Euler characteristic of the sphere, i.e., $N_V - N_E + N_F = 2$ (number of vertices, edges, and faces), can in principle be prepared using triangular NDs.

DOI: 10.1021/acsomega.8b01445
ACS Omega 2018, 3, 10631−10637

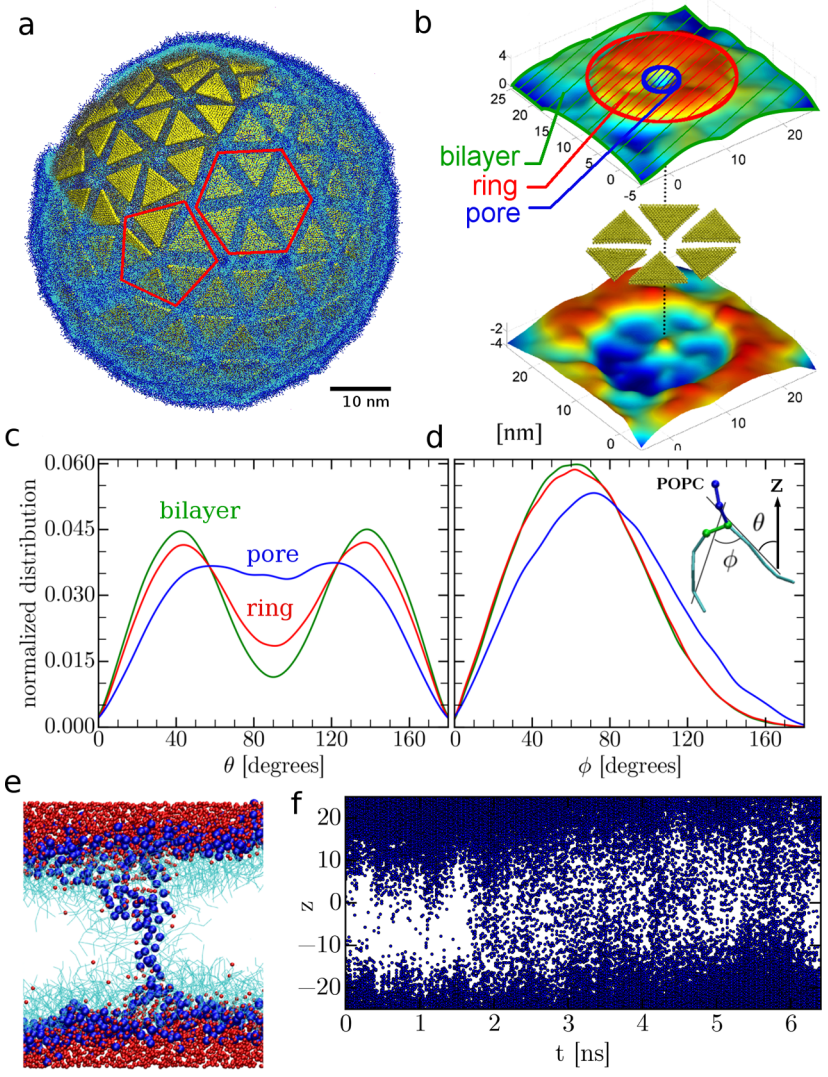

Figure 3. Stabilization of NDs with $\alpha = 1$ intercalated within spherical and planar POPC bilayers. (a) Hybrid NP−liposome ($d \approx 30$ nm) with 180 intercalated triangular NDs and 36 748 lipid molecules solvated in 2 669 168 water beads after 150 ns equilibration. A portion of the lipids at the top is hidden to show better the NDs organization. Representative 5 (pentagon) and 6 (hexagon) ND clusters are marked. (b) A cluster of such 6 triangular NDs inside a POPC bilayer, equilibrated for 200 ns. A color map surface is fitted to the polar heads of the lipid molecules to show the bilayer structure. (c, d) Normalized distributions of an azimuthal tilt angle and an angle between hydrophobic tails of POPC lipid molecules in the pore, ND ring, and bilayer regions, shown in (b). (e) Side view of a central portion of the pore, showing water molecules in red and polar head group of lipids in blue. (f) Fluctuations of water beads within the pore region.

Liposomes intercalated with NDs, such as shown in Figure 3a, can have unique features and applications. Partial equilibration of this hybrid NP−liposome ($\alpha = 1$) for 150 ns shows a significant annihilation of defects, present in the initial configuration, which leads to an overall stabilization of the whole superstructure. The intercalated NDs do not disturb much the lipid vesicle stability, since its fluidic lipid double layer naturally seals off small gaps and holes initially present between the NDs. However, it turns out that healing of holes is not complete for the current thickness and shape of nanoplates. One can observe a transient formation and disappearance of water chains in nanopores between the NDs tips, which are only partially filled with lipids and the associated opening and closure of the nanopore. These pores might allow the exchange of molecules between the interior and exterior of the NP−liposome, as in NPs capsules.[28]

Figure 3b shows a standalone nanopore formed between 6 NDs intercalated within a flat POPC bilayer (≈29.2 × 29.2 nm^2) and simulated for ≈200 ns. Although this single-pore system is flat, the pore should have similar characteristics, like nanopores present in the above hybrid spherical liposome. The colored surface in Figure 3b clearly shows that the pore of ≈2 nm in diameter is formed along a vertical axis within a ring structure of 6 NDs. A cross-section snapshot of the pore region, displayed in Figure 3e, reveals a large tilting of lipids taking part during their wrapping around the NDs. In the confined geometry of 6 nearby NDs, lipids form a cylindrical structure, with their polar heads arranged in the center along the vertical axis of the cylindrical pore, attracting thus water molecules.

To quantify an average configuration of lipids present within the pore, we first analyze their orientation in the bilayer, ring, and pore regions specified in Figure 3b. Two angles, θ and ϕ, are defined to measure the overall tilt angle of a lipid molecule from the vertical z-axis and the spread angle between its two hydrophobic tails, respectively (see inset of Figure 3d). The

DOI: 10.1021/acsomega.8b01445
ACS Omega 2018, 3, 10631−10637

angular distributions present in Figure 3c,d show that lipids in the ring structure, directly above and below the NDs, have an orientation that is similar to a normal lipid bilayer with $\theta = 40°$ and $\phi = 60°$. However, lipids in the pore region have a very different orientation. These lipids are significantly tilted with a wide range of tilt angles ($\theta = 60-120°$) and the hydrophobic tails within each lipid are relatively well separated ($\phi = 70°$).

Our simulations reveal the formation of 1−2 water chains within the pore region. Once formed, the nanopores are stable within the simulation time scale, however, the passage of water through the nanopore is fluctuating. These water chains are typically one-molecule wide but can also be two-molecule wide. To quantify the pore dynamics and its potential for a molecular transport, we monitor the presence of water inside the interstitial region between 6 NDs. Figure 3f shows a time-dependent water filling of the pore by revealing the z-positions of all water CG beads with respective to the middle plane of the bilayer. We can identify the formation of transient water chains occasionally passing for a few picoseconds through the whole pore region. Therefore, we can see that the aligned polar heads in the center of the pore could facilitate the transport of water and other solvated molecules. Similar exchange of molecules can be anticipated between the interior and exterior of a hybrid NP−liposome, shown in Figure 3a.

3. COMPUTATIONAL METHODS

We study the NP−lipid systems using CGMD simulations with the MARTINI force field,[66] where roughly every four nonhydrogen atoms and hydrogen atoms coupled to them are mapped onto a CG bead (see Table 1). The bonded and nonbonded interactions between CG beads are parameterized based on the MARTINI 2.0 force field,[67] where the bonded interactions between beads are described using harmonic potentials and the nonbonded interactions between beads are described using Lennard-Jones (LJ) potentials

$$V_{LJ}(r) = 4\epsilon\left\{\left(\frac{\sigma}{r}\right)^{12} - \left(\frac{\sigma}{r}\right)^{6}\right\} \quad (1)$$

where σ is the effective minimum distance between two beads (zero-crossing point of the potential) and ϵ is the strength of their interaction.

The gold NP core (d = 1.6 nm) is formed by 55 SC_4-type CG beads arranged into a cuboctahedral shape of a face-centered cubic lattice structure. The bonding distance between these beads is 4.08 Å, which is the lattice constant of bulk gold. This structure is maintained by relatively rigid bonds (15 kcal/(mol Å^2)) and SC_4−SC_4−SC_4 angles (60°, 2.988 kcal/(mol rad^2)). In a similar way, triangular nanodiscs (ND) are modeled using SC_4-type CG beads arranged into a hexagonal close-packed lattice structure. Dodecanethiol ligands are attached onto all CG beads that are on the NP surface. Each ligand is represented as a linear chain of three apolar C_1S-type CG beads, with parameters of saturated carbon chains (C_1-type) from the MARTINI force field, since they are chemically similar to the hydrophobic tails of lipid molecules. In this model, the interactions between NP ligands are assumed to be dominant, such that the interactions between NP cores are neglected. This is a valid assumption for NPs with a normal-to-high ligand density.[63,68] Therefore, the coupling strength between neighboring NPs is controlled by the strength of nonbonded interaction between C_1S CG beads.

The lipid bilayer is prepared from 1-palmitoyl-2-oleoyl-*sn*-glycero-3-phosphocholine (POPC) molecules. The amine head groups, phosphate head groups, and hydrophobic tails of the POPC molecules are modeled using Q_0-type, Q_a-type, and C_1-type CG beads, respectively. These POPC molecules are also used to form a micelle enclosure for the solvation of hydrophobic NPs in water. The lipid bilayer is solvated in water (P_4-type CG beads), with one antifreezing molecule (BP_4-type CG bead) added to every 9 water beads to prevent the undesirable crystallization of water at 310 K, formed due to the simplified description of water molecules in the MARTINI force field.[67] BP_4-type beads are modified P_4-type beads with σ = 5.7 Å for the BP_4−P_4 LJ coupling.

The CGMD simulations are performed with the nanoscale molecular dynamics software[69−71] in an isobaric-isothermal (NPT) ensemble. A barostat pressure of P = 1 atm is maintained by the Langevin piston method,[72] with a decay period of 200 fs and a damping coefficient of 50 fs. A Langevin thermostat is set to T = 310 K, with a damping coefficient of 1 ps^{-1} and a timestep of t = 20 fs.

Table 1. Definition of CG Beads Used in the Model[a]

bead-type	representation	chemical nature
SC_4	four gold atoms (NP core)	N/A
C_1S	four methylene (NP ligand)	nonpolar
Q_0	choline	charged
Q_a	phosphate	charged
N_a	glycerol	nonpolar
C_1	hydrocarbon	nonpolar
P_4	four water molecules	polar
BP_4	anti-freeze	polar

[a] Q_0, Q_a, N_a, and C_1 are defined in the MARTINI force field.

4. CONCLUSIONS

We have investigated the insertion, stabilization, structure, and dynamics of small hydrophobic NPs and their clusters inside lipid bilayers of planar and spherical shapes. The insertion dynamics is controlled by lipid coverage around the NP. Less protected NPs are less soluble in water and therefore have a faster insertion into the lipid bilayers. The equilibrium structures of NP clusters formed inside lipid bilayers are correlated with the relative coupling strength between the NP ligands and lipids. Hybrid structures of NDs intercalated within liposomes are also simulated. We observed the formation of nanopores between 6 NDs intercalated within lipid bilayers, allowing a transient passage of water. These simulation results provide insights into the complex but intriguing co-assembly behavior of NPs with lipid bilayers. We envision this study to inspire future studies that can potentially look into the insertion mechanisms of shaped NPs, such as triangular NDs, and the effect of size polydispersity in pore formation.

AUTHOR INFORMATION

Corresponding Authors

*E-mail: hchan@anl.gov (H.C.).
*E-mail: pkral@uic.edu (P.K.).

ORCID

Henry Chan: 0000-0002-8198-7737
Petr Král: 0000-0003-2992-9027

DOI: 10.1021/acsomega.8b01445
ACS Omega 2018, 3, 10631−10637

Present Address

[‖]Center for Nanoscale Materials, Argonne National Laboratory, 9700 Cass Avenue, Lemont, Illinois 60439, United States (H.C.).

Notes

The authors declare no competing financial interest.

■ ACKNOWLEDGMENTS

We acknowledge Dr. Alexey Titov for his contributions to the work and the support of the NSF DMR-1506886 award.

■ REFERENCES

(1) Kushner, D. J. Self-assembly of biological structures. *Bacteriol. Rev.* **1969**, *33*, 302.

(2) Zhang, S. Building from the bottom up. *Mater. Today* **2003**, *6*, 20−27.

(3) He, J.; Liu, Y.; Babu, T.; Wei, Z.; Nie, Z. Self-assembly of inorganic nanoparticle vesicles and tubules driven by tethered linear block copolymers. *J. Am. Chem. Soc.* **2012**, *134*, 11342−11345.

(4) Miszta, K.; de Graaf, J.; Bertoni, G.; Dorfs, D.; Brescia, R.; Marras, S.; Ceseracciu, L.; Cingolani, R.; van Roij, R.; Dijkstra, M.; Manna, L. Hierarchical self-assembly of suspended branched colloidal nanocrystals into superlattice structures. *Nat. Mater.* **2011**, *10*, 872−876.

(5) Zhu, C.; Guo, S.; Zhai, Y.; Dong, S. Layer-by-layer self-assembly for constructing a graphene/platinum nanoparticle three-dimensional hybrid nanostructure using ionic liquid as a linker. *Langmuir* **2010**, *26*, 7614−7618.

(6) Szabó, Z.; Cora, I.; Horváth, Z.; Volk, J.; Baji, Z. Hierarchical oxide nanostructures fabricated with atomic layer deposition and hydrothermal growth. *Nano-Struct. Nano-Objects* **2018**, *13*, 100−108.

(7) King'ondu, C. K.; Garces, H. F.; Suib, S. L. End-to-end and side-by-side alignment of short octahedral molecular sieve (OMS-2) nanorods into long microyarn superarchitectures and highly flexible membranes. *Nano-Struct. Nano-Objects* **2018**, *14*, 49−56.

(8) Titov, A. V.; Král, P.; Pearson, R. Sandwiched Graphene-Membrane Superstructures. *ACS Nano* **2010**, *4*, 229−234.

(9) Boissiere, C.; Grosso, D.; Chaumonnot, A.; Nicole, L.; Sanchez, C. Aerosol route to functional nanostructured inorganic and hybrid porous materials. *Adv. Mater.* **2011**, *23*, 599−623.

(10) Webb, C. The body shops. *IEEE Spectrum* **2005**, *42*, 34−39.

(11) Auyeung, E.; Li, T. I.; Senesi, A. J.; Schmucker, A. L.; Pals, B. C.; de La Cruz, M. O.; Mirkin, C. A. DNA-mediated nanoparticle crystallization into Wulff polyhedra. *Nature* **2014**, *505*, 73−77.

(12) Gupta, S.; Wood, R. Development of FRET biosensor based on aptamer/functionalized graphene for ultrasensitive detection of bisphenol A and discrimination from analogs. *Nano-Struct. Nano-Objects* **2017**, *10*, 131−140.

(13) Hindumathi, R.; Jagannatham, M.; Haridoss, P.; Sharma, C. P. Novel nano-cocoon like structures of polyethylene glycol-multiwalled carbon nanotubes for biomedical applications. *Nano-Struct. Nano-Objects* **2018**, *13*, 30−35.

(14) Cheng, X.; Pan, F.; Wang, M.; Li, W.; Song, Y.; Liu, G.; Yang, H.; Gao, B.; Wu, H.; Jiang, Z. Hybrid membranes for pervaporation separations. *J. Membr. Sci.* **2017**, *541*, 329−346.

(15) Häffner, S. M.; Malmsten, M. Membrane interactions and antimicrobial effects of inorganic nanoparticles. *Adv. Colloid Interface Sci.* **2017**, *248*, 105−128.

(16) Rasch, M. R.; Rossinyol, E.; Hueso, J. L.; Goodfellow, B. W.; Arbiol, J.; Korgel, B. A. Hydrophobic Gold Nanoparticle Self-Assembly with Phosphatidylcholine Lipid: Membrane-Loaded and Janus Vesicles. *Nano Lett.* **2010**, *10*, 3733−3739.

(17) Chen, Y.; Bose, A.; Bothun, G. D. Controlled Release from Bilayer-Decorated Magnetoliposomes via Electromagnetic Heating. *ACS Nano* **2010**, *4*, 3215−3221.

(18) Bonnaud, C.; Monnier, C. A.; Demurtas, D.; Jud, C.; Vanhecke, D.; Montet, X.; Hovius, R.; Lattuada, M.; Rothen-Rutishauser, B.; Petri-Fink, A. Insertion of particle clusters into vesicle bilayers. *ACS Nano* **2014**, *8*, 3451−3460.

(19) Reimhult, E. Nanoparticle-triggered release from lipid membrane vesicles. *New Biotechnol.* **2015**, *32*, 665−672.

(20) Jing, B.; Zhu, Y. Disruption of supported lipid bilayers by semihydrophobic nanoparticles. *J. Am. Chem. Soc.* **2011**, *133*, 10983−10989.

(21) Leroueil, P. R.; Berry, S. A.; Duthie, K.; Han, G.; Rotello, V. M.; McNerny, D. Q.; Baker, J. R.; Orr, B. G.; Holl, M. M. B. Wide varieties of cationic nanoparticles induce defects in supported lipid bilayers. *Nano Lett.* **2008**, *8*, 420−424.

(22) Pogodin, S.; Werner, M.; Sommer, J.-U.; Baulin, V. A. Nanoparticle-Induced Permeability of Lipid Membranes. *ACS Nano* **2012**, *6*, 10555−10561.

(23) Song, B.; Yuan, H.; Pham, S. V.; Jameson, C. J.; Murad, S. Nanoparticle Permeation Induces Water Penetration, Ion Transport, and Lipid Flip-Flop. *Langmuir* **2012**, *28*, 16989−17000.

(24) Paasonen, L.; Sipilä, T.; Subrizi, A.; Laurinmäki, P.; Butcher, S. J.; Rappolt, M.; Yaghmur, A.; Urtti, A.; Yliperttula, M. Gold-embedded photosensitive liposomes for drug delivery: Triggering mechanism and intracellular release. *J. Controlled Release* **2010**, *147*, 136−143.

(25) Santhosh, P. B.; Penič, S.; Genova, J.; Iglič, A.; Kralj-Iglič, V.; Ulrih, N. P. A study on the interaction of nanoparticles with lipid membranes and their influence on membrane fluidity. *J. Phys.: Conf. Ser.* **2012**, *398*, No. 012034.

(26) Lai, K.; Wang, B.; Zhang, Y.; Zheng, Y. Computer simulation study of nanoparticle interaction with a lipid membrane under mechanical stress. *Phys. Chem. Chem. Phys.* **2013**, *15*, 270−278.

(27) Rascol, E.; Devoisselle, J.-M.; Chopineau, J. The relevance of membrane models to understand nanoparticles-cell membrane interactions. *Nanoscale* **2016**, *8*, 4780−4798.

(28) Yang, M.; Chan, H.; Zhao, G.; Bahng, J. H.; Zhang, P.; Král, P.; Kotov, N. A. Self-assembly of nanoparticles into biomimetic capsid-like nanoshells. *Nat. Chem.* **2017**, *9*, 287.

(29) Lin, G.; Chee, S. W.; Raj, S.; Král, P.; Mirsaidov, U. Linker-mediated self-assembly dynamics of charged nanoparticles. *ACS Nano* **2016**, *10*, 7443−7450.

(30) da Rocha, E. L.; Caramori, G. F.; Rambo, C. R. Nanoparticle translocation through a lipid bilayer tuned by surface chemistry. *Phys. Chem. Chem. Phys.* **2013**, 2282−2290.

(31) Ding, H.-m.; Tian, W.-d.; Ma, Y.-q Designing Nanoparticle Translocation through Membranes by Computer Simulations. *ACS Nano* **2012**, *6*, 1230−1238.

(32) Yang, K.; Ma, Y.-Q. Computer simulation of the translocation of nanoparticles with different shapes across a lipid bilayer. *Nat. Nanotecnol.* **2010**, *5*, 579−583.

(33) Li, Y.; Chen, X.; Gu, N. Computational Investigation of Interaction between Nanoparticles and Membranes: Hydrophobic/Hydrophilic Effect. *J. Phys. Chem. B* **2008**, *112*, 16647−16653.

(34) Wong-Ekkabut, J.; Baoukina, S.; Triampo, W.; Tang, I.-M.; Tieleman, D. P.; Monticelli, L. Computer simulation study of fullerene translocation through lipid membranes. *Nat. Nanotechnol.* **2008**, *3*, 363−368.

(35) Barnoud, J.; Rossi, G.; Monticelli, L. Lipid membranes as solvents for carbon nanoparticles. *Phys. Rev. Lett.* **2014**, *112*, No. 068102.

(36) Jackson, A. M.; Myerson, J. W.; Stellacci, F. Spontaneous assembly of subnanometre-ordered domains in the ligand shell of monolayer-protected nanoparticles. *Nat. Mater.* **2004**, *3*, 330−336.

(37) Simonelli, F.; Bochicchio, D.; Ferrando, R.; Rossi, G. Monolayer-Protected Anionic Au Nanoparticles Walk into Lipid Membranes Step by Step. *J. Phys. Chem. Lett.* **2015**, *6*, 3175−3179.

(38) Verma, A.; Uzun, O.; Hu, Y. H.; Hu, Y.; Han, H. S.; Watson, N.; Chen, S. L.; Irvine, D. J.; Stellacci, F. Surface-structure-regulated cell-membrane penetration by monolayer-protected nanoparticles. *Nat. Mater.* **2008**, *7*, 588−595.

(39) Van Lehn, R. C.; Ricci, M.; Silva, P. H.; Andreozzi, P.; Reguera, J.; Voïtchovsky, K.; Stellacci, F.; Alexander-Katz, A. Lipid tail

DOI: 10.1021/acsomega.8b01445
ACS Omega 2018, 3, 10631−10637

protrusions mediate the insertion of nanoparticles into model cell membranes. *Nat. Commun.* **2014**, *5*, No. 4482.
(40) Van Lehn, R. C.; Alexander-Katz, A. Pathway for insertion of amphiphilic nanoparticles into defect-free lipid bilayers from atomistic molecular dynamics simulations. *Soft Matter* **2015**, *11*, 3165−3175.
(41) Van Lehn, R. C.; Alexander-Katz, A. Free energy change for insertion of charged, monolayer-protected nanoparticles into lipid bilayers. *Soft Matter* **2014**, *10*, 648−658.
(42) Van Lehn, R. C.; Atukorale, P. U.; Carney, R. P.; Yang, Y.-S.; Stellacci, F.; Irvine, D. J.; Alexander-Katz, A. Effect of Particle Diameter and Surface Composition on the Spontaneous Fusion of Monolayer-Protected Gold Nanoparticles with Lipid Bilayers. *Nano Lett.* **2013**, *13*, 4060−4067.
(43) Van Lehn, R. C.; Alexander-Katz, A. Fusion of Ligand-Coated Nanoparticles with Lipid Bilayers: Effect of Ligand Flexibility. *J. Phys. Chem. A* **2014**, *118*, 5848−5856.
(44) Van Lehn, R. C.; Alexander-Katz, A. Penetration of lipid bilayers by nanoparticles with environmentally-responsive surfaces: simulations and theory. *Soft Matter* **2011**, *7*, 11392−11404.
(45) Šarić, A.; Cacciuto, A. Self-assembly of nanoparticles adsorbed on fluid and elastic membranes. *Soft Matter* **2013**, *9*, 6677−6695.
(46) Gorgoll, R. M.; Tsubota, T.; Harano, K.; Nakamura, E. Cooperative self-assembly of gold nanoparticles on the hydrophobic surface of vesicles in water. *J. Am. Chem. Soc.* **2015**, *137*, 7568−7571.
(47) Angelikopoulos, P.; Sarkisov, L.; Cournia, Z.; Gkeka, P. Self-assembly of anionic, ligand-coated nanoparticles in lipid membranes. *Nanoscale* **2017**, *9*, 1040−1048.
(48) Binder, W. H.; Sachsenhofer, R.; Farnik, D.; Blaas, D. Guiding the location of nanoparticles into vesicular structures: a morphological study. *Phys. Chem. Chem. Phys.* **2007**, *9*, 6435−6441.
(49) Gopalakrishnan, G.; Danelon, C.; Izewska, P.; Prummer, M.; Bolinger, P.-Y.; Geissbühler, I.; Demurtas, D.; Dubochet, J.; Vogel, H. Multifunctional Lipid/Quantum Dot Hybrid Nanocontainers for Controlled Targeting of Live Cells. *Angew. Chem., Int. Ed.* **2006**, *45*, 5478−5483.
(50) Rasch, M. R.; Yu, Y.; Bosoy, C.; Goodfellow, B. W.; Korgel, B. A. Chloroform-Enhanced Incorporation of Hydrophobic Gold Nanocrystals into Dioleoylphosphatidylcholine (DOPC) Vesicle Membranes. *Langmuir* **2012**, *28*, 12971−12981.
(51) Bothun, B. Hydrophobic silver nanoparticles trapped in lipid bilayers: Size distribution, bilayer phase behavior, and optical properties. *J. Nanobiotechnol.* **2008**, *6*, 13.
(52) Chan, H.; Král, P. Self-standing nanoparticle membranes and capsules. *Nanoscale* **2011**, *3*, 1881−1886.
(53) He, J.; Lin, X.-M.; Chan, H.; Vuković, L.; Král, P.; Jaeger, H. M. Diffusion and Filtration Properties of Self-Assembled Gold Nanocrystal Membranes. *Nano Lett.* **2011**, *11*, 2430−2435.
(54) Bera, M. K.; Chan, H.; Moyano, D. F.; Yu, H.; Tatur, S.; Amoanu, D.; Bu, W.; Rotello, V. M.; Meron, M.; Král, P.; Lin, B.; Schlossman, M. L. Interfacial Localization and Voltage-Tunable Arrays of Charged Nanoparticles. *Nano Lett.* **2014**, *14*, 6816−6822.
(55) Guo, Y.; Terazzi, E.; Seemann, R.; Fleury, J. B.; Baulin, V. A. Direct proof of spontaneous translocation of lipid-covered hydrophobic nanoparticles through a phospholipid bilayer. *Sci. Adv.* **2016**, *2*, No. e1600261.
(56) Marrink, S. J.; Mark, A. E. The mechanism of vesicle fusion as revealed by molecular dynamics simulations. *J. Am. Chem. Soc.* **2003**, *125*, 11144−11145.
(57) Marsh, D. Lateral Pressure Profile, Spontaneous Curvature Frustration, and the Incorporation and Conformation of Proteins in Membranes. *Biophys. J.* **2007**, *93*, 3884−3899.
(58) Gullingsrud, J.; Schulten, K. Lipid Bilayer Pressure Profiles and Mechanosensitive Channel Gating. *Biophys. J.* **2004**, *86*, 3496−3509.
(59) Andersen, O. S.; Koeppe, R. E. Bilayer Thickness and Membrane Protein Function: An Energetic Perspective. *Annu. Rev. Biophys. Biomol. Struct.* **2007**, *36*, 107−130.
(60) Paik, T.; Gordon, T. R.; Prantner, A. M.; Yun, H.; Murray, C. B. Designing Tripodal and Triangular Gadolinium Oxide Nanoplates and Self-Assembled Nanofibrils as Potential Multimodal Bioimaging Probes. *ACS Nano* **2013**, *7*, 2850−2859.
(61) Chen, L.; Ji, F.; Xu, Y.; He, L.; Mi, Y.; Bao, F.; Sun, B.; Zhang, X.; Zhang, Q. High-yield seedless synthesis of triangular gold nanoplates through oxidative etching. *Nano Lett.* **2014**, *14*, 7201−7206.
(62) Talapin, D. V.; Nelson, J. H.; Shevchenko, E. V.; Aloni, S.; Sadtler, B.; Alivisatos, A. P. Seeded Growth of Highly Luminescent CdSe/CdS Nanoheterostructures with Rod and Tetrapod Morphologies. *Nano Lett.* **2007**, *7*, 2951−2959.
(63) Titov, A. V.; Král, P. Modeling the Self-Assembly of Colloidal Nanorod Superlattices. *Nano Lett.* **2008**, *8*, 3605−3612.
(64) Baker, J. L.; Widmer-Cooper, A.; Toney, M. F.; Geissler, P. L.; Alivisatos, A. P. Device-Scale Perpendicular Alignment of Colloidal Nanorods. *Nano Lett.* **2010**, *10*, 195−201.
(65) Yeom, J.; Yeom, B.; Chan, H.; Smith, K. W.; Dominguez-Medina, S.; Bahng, J. H.; Zhao, G.; Chang, W.-S.; Chuvilin, A.; Melnikau, D.; Rogach, A. L.; Zhang, P.; Link, S.; Král, P.; Kotov, N. A. Chiral templating of Self-assembling nanostructures by cicircular polarized light. *Nat. Mater.* **2015**, *14*, 66−72.
(66) Marrink, S. J.; de Vries, A. H.; Mark, A. E. Coarse Grained Model for Semiquantitative Lipid Simulations. *J. Phys. Chem. B* **2004**, *108*, 750−760.
(67) Marrink, S. J.; Risselada, H. J.; Yefimov, S.; Tieleman, D. P.; de Vries, A. H. The MARTINI Force Field: Coarse Grained Model for Biomolecular Simulations. *J. Phys. Chem. B* **2007**, *111*, 7812−7824.
(68) Talapin, D. V.; Shevchenko, E. V.; Murray, C. B.; Titov, A. V.; Král, P. Dipole-Dipole Interactions in Nanoparticle Superlattices. *Nano Lett.* **2007**, *7*, 1213−1219.
(69) Phillips, J. C.; Braun, R.; Wang, W.; Gumbart, J.; Tajkhorshid, E.; Villa, E.; Chipot, C.; Skeel, R. D.; Kalé, L.; Schulten, K. Scalable molecular dynamics with NAMD. *J. Comput. Chem.* **2005**, *26*, 1781−1802.
(70) Humphrey, W.; Dalke, A.; Schulten, K. VMD: Visual molecular dynamics. *J. Mol. Graphics* **1996**, *14*, 33−38.
(71) Shih, A. Y.; Freddolino, P. L.; Arkhipov, A.; Schulten, K. Assembly of lipoprotein particles revealed by coarse-grained molecular dynamics simulations. *J. Struct. Biol.* **2007**, *157*, 579−592.
(72) Feller, S. E.; Zhang, Y.; Pastor, R. W.; Brooks, B. R. Constant pressure molecular dynamics simulation: The Langevin piston method. *J. Chem. Phys.* **1995**, *103*, 4613−4621.

DOI: 10.1021/acsomega.8b01445
ACS Omega 2018, 3, 10631−10637